Bull Earthquake Eng (2007) 5:27–43
DOI 10.1007/s10518-006-9026-x

ORIGINAL RESEARCH PAPER

Characteristics of strong ground motion data recorded in the Gubbio sedimentary basin (Central Italy)

F. Pacor · D. Bindi · L. Luzi · S. Parolai · S. Marzorati · G. Monachesi

Received: 18 November 2005 / Accepted: 12 September 2006 /
Published online: 27 October 2006

Abstract Various authors, analysing the set of accelerograms recorded at Gubbio Piana (GBP) (central Italy), have demonstrated that strong amplification occurs at this accelerometric station, which is installed within an alluvial basin. In particular, Ambraseys et al. [(2005a), Bull Earthq Eng 3:1–53; (2005b), Bull Earth Eng 3:55–73] observed that the strong motion peaks at GBP greatly exceed the median values predicted by the attenuation relationships they derived for Europe. In this work, we analyse and discuss some characteristics of the ground motion recorded at the GBP station. We show that the ground motion parameters, such as peak-ground acceleration and peak-ground velocity, are strongly influenced by the presence of locally induced surface waves that produce both a lengthening of the significant shaking duration and an increase in the peak values with respect to a nearby bedrock site. The basin-induced surface waves are observed in the three components of motion and their effects on the peak values are particularly evident in the vertical component. In the frequency domain, the energy of the surface waves is mostly restricted to the frequency band 0.4–0.8 Hz for both the horizontal and vertical components. The horizontal and vertical Fourier amplitudes are also very similar, and this indicates that the H/V spectral ratio technique is not applicable to describing the site response due to the propagation of seismic wave in a complex 2D/3D geological structure. Finally, a preliminary polarization analysis shows that the directions of polarization, as well

F. Pacor · D. Bindi (✉) · L. Luzi · S. Marzorati
Istituto Nazionale di Geofisica e Vulcanologia,
Via Bassini 15, 20133 Milano, Italy
e-mail: bindi@mi.ingv.it

S. Parolai
GeoForschungsZentrum Potsdam, Telegrafenberg,
14473 Potsdam, Germany

G. Monachesi
Istituto Nazionale di Geofisica e Vulcanologia,
Via di Vigna Murata 605, 00143 Roma, Italy

as the degree of elliptical polarization, exhibit a strong variability with time, that may be related to a complex propagation of Love and Rayleigh waves within the basin.

Keywords Strong motion · Alluvial basin effects · Site effects · Gubbio plain

1 Introduction

This work was motivated by the similar results presented by a number of authors (Castro et al. 2004; Bindi et al. 2004, 2006, Luzi et al. 2005; Ambraseys et al. 2005a; Ambraseys et al. 2005b) concerning the strong amplification observed at the Gubbio Piana (GBP) accelerometric station (central Italy), installed within an alluvial basin. The origin of the amplification can be ascribed to the basin edge structure and to the geophysical characteristics of the sedimentary layers, since the recordings of the nearby bedrock site Gubbio (GBB) differ in amplitude and frequency content. Several recent studies (e.g. Graves et al. 1998, Chavez-Garcia and Faccioli 2000, Olsen 2000, Makra et al. 2001, Hurby and Beresnev 2003, Choi et al. 2005) have showed that ground motion within sedimentary basins is strongly influenced by the interaction between the incoming body waves and the 2D/3D structure of a basin's edge. For example, the lengthening of the shake duration due to basin-edge effects is well documented (e.g. Joyner 2000).

The strong motion data recorded during the 1997–1998 Umbria Marche seismic sequence (SSN 2002) were used by several authors (e.g. Castro et al. 2004; Bindi et al. 2004; Luzi et al. 2005)) to compute the site transfer functions of some accelerometric stations in central Italy. The transfer functions were obtained by applying the generalized inversion technique (Castro et al. 1990), that provides the frequency dependent site amplification with respect to the site amplification of a reference station. The results found by these authors showed that GBB displays amplifications in the range 2–10 Hz that never exceed a value of 4. By contrast, significant amplifications (up to 20) occur at GBP in the low frequency range (<1 Hz) for both the vertical and horizontal components. Luzi et al. (2005) compared the GBP transfer function with theoretical models computed considering both a 1D vertically layered medium and a simplified 2D model for the Gubbio plain. In the former case, the authors applied the Haskell–Thomson propagation matrix approach (Haskell 1953, Thomson 1950) to estimate the 1D transfer function, while the indirect boundary element method (Sanchez-Sesma et al. 1993) was applied to study the 2D effects, considering a simplified basin-edge model having a trapezoidal shape and a sedimentary cover composed of a single elastic layer over the bedrock. Their results (Luzi et al. 2005, Figure 13) showed that 2D effects play a fundamental role in determining the amplitude and phase of the horizontal and vertical transfer functions of GBP.

Recently, Ambraseys et al. (2005a), Ambraseys et al. (2005b) derived new attenuation relationships for horizontal and vertical peak ground acceleration (PGA) and spectral acceleration (SA), mainly using recordings from four European countries (Italy, Greece, Turkey and Iceland). Most of the Italian recordings were associated with two earthquakes, the 15 September 1976 ($M_w = 6$) Friuli earthquake and the 23 November 1980 ($M_w = 6.9$) Irpinia earthquake. They also used the September 1997–April 1998 Umbria-Marche seismic sequence (with the strongest shock having $M_w = 6$). In particular, three of the earthquakes that occurred during the Umbria-Marche sequence are amongst the best-recorded events (13 records or more) in the

analysed data set (Ambraseys et al. 2005a, Table 4, p30). The authors observed that some Italian stations exhibited peaks of ground motion that significantly deviate from the predicted median values, including GBP which showed a median amplification of 8.16 at a natural period of 2 s (Ambraseys et al. 2005a, Table 3, p29). Recently, Bindi et al. (2006) exploited the strong-motion acceleration data set of the 1997–1998 Umbria-Marche sequence (SSN 2002) to derive regional attenuation relationships for the area (hereinafter referred to as UMA05), and again showed how ground motion at GBP is systematically larger than the predictions. Both, Ambraseys et al. (2005a) and Bindi et al. (2006), consistent with Luzi et al. (2005), suggest that the considerable amplification in the recordings at GBP may be due to long-period surface waves generated at the edge of the sedimentary basin.

Since ground-motion amplifications like those observed at GBP were observed at other stations installed in similar sedimentary basins in central Italy (Castro et al. 2004, Luzi et al. 2005, Bindi et al. 2006), an understanding of this phenomenon, as suggested by Ambraseys et al. (2005a), Ambraseys et al. (2005b), is also necessary to identify which characteristics make a site not suitable for inclusion when deriving attenuation relationships that are valid to at least an average European level. With this aim, we analyse in the time and frequency domain the strong ground motions recorded by GBP and GBB accelerometric stations, compute the peak and integral ground-motion parameters and compare them with the values predicted by regional attenuation relationships. Similarly to Diallo et al. (2005), spectral analysis and multi-component polarisation analyses are performed on the GBP recordings to identify the frequency content of the different phases composing the recorded wavefield and to highlight the importance of basin-induced surface waves in modifying the main strong ground-motion parameters.

2 Geological setting

The inner sector of the Tuscan and Umbria-Marche Apennines has been affected by an extensional tectonic regime since the Miocene. This tectonic phase is responsible for the creation of a series of *en echelon* basins having a general NW–SE trend, formed by normal faults with a dislocation of several thousand meters. These tectonic depressions are generally filled with continental deposition facies.

The Gubbio basin is located along a NW–SE trend for a length of about 20 km, with a width reaching 4 km (Fig. 1). The basin was formed by a 120°–150° striking, 50°–70° dipping normal fault, whose plane emerges on the western edge of the depression that lowered the SW flank of a calcareous anticline (Collettini et al. 2003, Pucci et al. 2003, Mirabella et al. 2004). The calcareous formation of the Umbria-Marche sequence and a flysch sequence, the "Formazione Marnoso-Arenacea", outcrop in the eastern and western side of the basin, respectively. The basin is filled by a sedimentary sequence of Pleistocenic origin. Deep boreholes, drilled by GE.MI.NA (1963) for mineral exploration, found that the sedimentary sequence reaches a maximum thickness of 400 m and consists of three main sedimentary units. These are, from bottom to top: (1) A clayey-lignitic basal complex, characterized by lignite layers interbedded with organic clays, and locally with sand and conglomerates, that can reach 200 m in thickness. This sequence can be found in the southern portion of the valley; (2) a clayey–sandy complex comprised of sand and sandy clay, interbedded with sandstone conglomerate lenses; (3) an upper alluvial complex, composed of slope debris, alluvial fan and

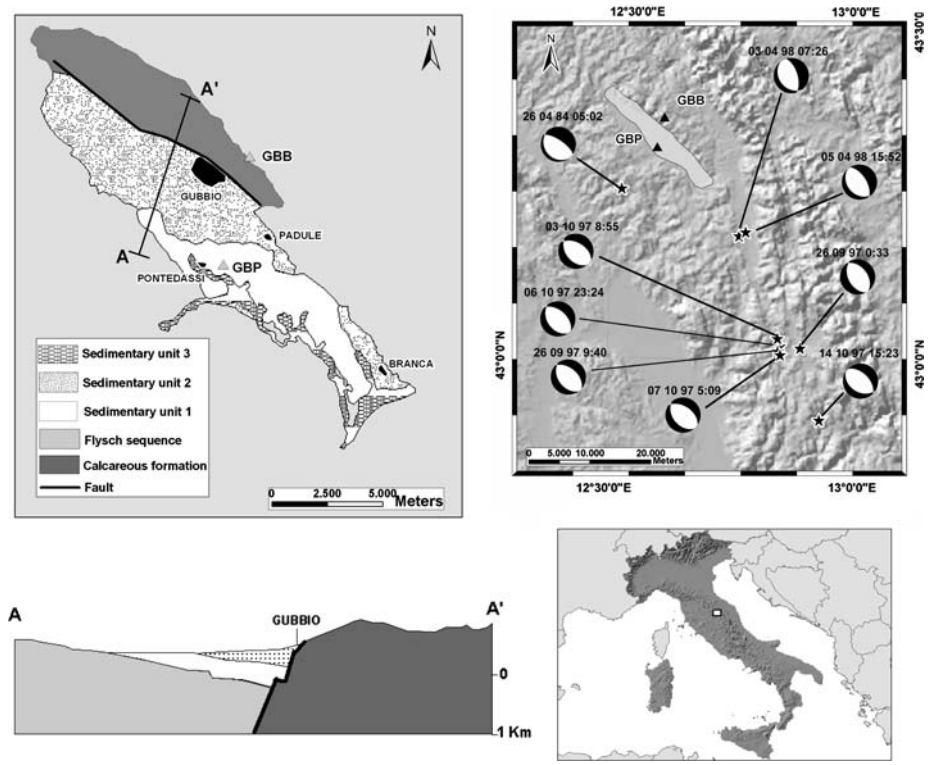

Fig. 1 *Left*: geological sketch of the Gubbio basin and a vertical cross section (simplified from Menichetti 1992). *Right*: the studied area, with the epicentres (stars) of the analysed earthquakes and locations of the Gubbio (GBB) and Gubbio Piana (GBP) stations (triangles). The focal mechanisms are also shown (Morelli et al. 2000)

fluvial deposits. A sketch of a geological cross section of the valley is shown in Fig. 1 (Menichetti 1992).

3 Strong motion data

The strong-motion data analysed in this study come from two accelerographs belonging to the Italian Strong Motion Network (RAN): the GBP station located inside the basin, which is equipped with a 12 bit digital instrument (Kinemetrics SSA1), while outside the valley, there is GBB station with an analog SMA-1 accelerograph installed on a rock site (Fig. 1). Both instruments are mounted on standard concrete pillars (SSN 2002).

The GBP station was triggered by eight earthquakes associated with the Umbria Marche seismic sequence (1997–1998) with $M > 4.5$, their epicenters marked in Fig. 1. Three of these events were also recorded by GBB (Table 1). The events had normal focal mechanisms and were located 20–50 km SSE of the sites with hypocentral depths in the range 2–10 km. The 1984 Gubbio earthquake ($M_1 = 5.2$), recorded only at GBB, completes the data-set. Table 1 lists the source parameters of the nine earthquakes

Table 1 *Left*: main epicentral and source parameters (Bindi et al. 2004) of the events recorded at the Gubbio (*GBB*) and Gubbio Piana (*GPB*) stations; *Right*: strong motion parameters estimated in the present study

EVENT	dd.mm.yy	hh:mm	lat.	long	MMe	H (km)	Mo (Nm)	STZ	R (Km)	PGA (cm/s^2)	PGV (cm/s)	Ia (cm/s)	T90 (s)	STZ	R (km)	PGA (cm/s^2)	PGV (cm/s)	Ia (cm/s)	T90 (s)
174	29.04.84	05:02	43.250	12.520	5.2	7.0	3.4×10^{17}	GBB	15.3	48.1	1.5	2.6	1.5						
										−66.4	−1.7	4.1	−1.7						
										−35.7	1.0	1.3	1.0						
290	26.09.97	00:33	43.021	12.888	5.6	3.8	4.0×10^{17}							GBP	38.8	−33.0	3.6	2.9	27.0
																−33.1	−3.7	2.6	29.4
																17.0	−3.0	1.4	31.9
286	26.09.97	09:40	43.023	12.847	5.9	6.5	1.2×10^{18}	GBB	42.9	61.2	−3.4	3.3	11.7	GBP	39.2	92.6	−13.9	23.3	29.7
										82.4	−2.9	3.7	11.5			−94.2	17.6	25.6	31.1
										−34.5	−2.4	1.3	12.0			64.9	13.4	15.5	22.1
350	03.10.97	08:55	43.034	12.842	5.4	5.7	8.6×10^{16}							GBP	37.6	48.8	−2.1	2.2	21.5
																46.0	−2.2	2.4	19.8
																−23.0	1.2	0.6	26.3
291	06.10.97	23:24	43.015	12.843	5.5	7.0	1.7×10^{17}	GBB	43.3	29.8	−1.3	1.0	8.5	GBP	39.6	72.3	4.0	6.7	17.6
										−39.0	−1.5	1.2	10.0			−58.1	4.8	5.7	20.9
										10.0	0.7	0.2	13.6			24.6	−3.1	1.6	27.5
353	07.10.97	05:09	43.010	12.848	4.8	10.0	6.7×10^{15}							GBP	40.9	−8.4	0.4	0.1	22.7
																11.4	−0.6	0.1	18.4
																5.9	−0.6	0.1	28.4
292	14.10.97	15:23	42.915	12.930	5.6	4.9	3.4×10^{17}							GBP	52.4	−14.3	−1.8	0.6	46.8
																−13.0	−2.0	0.6	36.4
																−7.4	1.1	0.3	48.5
364	03.04.98	07:26	43.184	12.759	5	2.6	5.7×10^{16}	GBB	23.2	26.6	2.0	0.6	7.0	GBP	20.0	−48.0	−4.0	4.3	16.7
										38.9	2.3	1.0	5.6			−44.7	−3.8	3.7	16.2
										15.9	0.9	0.2	8.5			26.1	1.6	1.2	19.5
365	05.04.98	15:52	43.190	12.773	4.7	5.4	1.9×10^{16}							GBP	20.9	−29.3	−2.2	1.2	18.0
																−22.7	−1.9	1.1	16.5
																14.8	1.2	0.4	19.1

R epicentral distance, *H* depth, *PGA* peak ground acceleration, *PGV* peak ground velocity, *Ia* Arias intensity, *T90* signal duration between which 5 and 95% of total energy was recorded. For each event, the first, second and third lines in the right part of the table correspond to the north–south, east–west and vertical components, respectively

used in this study, as well as the main strong-motion parameters observed at the two recording stations. These parameters have been evaluated only after the instrumental response was removed and the accelerometric records corrected for the base-line. In addition, the records have been re-sampled at 200 samples per second to obtain a uniform sampling rate. Finally, the records were filtered to remove the high- and low-frequency noise, by visually selecting a frequency interval of most use to this work. The average range used in this study was 0.4–20 Hz for GBB and 0.2–40 Hz for GBP.

4 Time domain analysis

Examples of acceleration, velocity and displacement time series recorded during the strongest events included in the data set are shown in Fig. 2a,b for GBP and GBB, respectively. We define the strong motion duration as the time interval (T_2–T_1) between which 5 and 95% of the total energy was recorded (Fig. 3a,b) for the GBP time series. Since at GBB the instrument is triggered by the S-wave arrival, T_1 coincides to 1% and T_2 to 91% of the total energy (Fig. 3c,d). However, since the triggering system is different for the analogic and digital stations, comparing the event duration at GBP and GBB is not straightforward. The strong-motion durations at GBP are 2 and 2.5 times longer than those recorded at GBB for horizontal and vertical components, respectively. The longer duration observed at GBP is due to the presence of low-frequency arrivals that are not found in the GBB records. For the strongest earthquakes ($M > 5$) these secondary phases have very large amplitudes, comparable to those of the S-waves. Figure 3a–d also show the normalized Arias intensity computed for event 286 (Table 1) considering the entire record and the 0.2–1.5 Hz pass band filtered signal. The frequency-dependence of the energy-time distribution computed for the two stations is very different: while at GBP more than 50% of cumulative energy is transported by low frequency waves, especially for the vertical component, the contribution of these arrivals at GBB is negligible to both components. This comparison provides evidence for the presence of locally induced low-frequency surface waves.

The PGA values observed at GBP are always larger than those recorded at GBB by a factor of about 1.7 for the horizontal, and two for the vertical, components. This ratio dramatically increases when the peak ground velocity (PGV) values are considered, reaching values of about 4 for both the components. The PGA values are generally observed corresponding to the S-wave arrivals, for both GBB and GBP, whereas the PGV and peak ground displacement (PGD) values at GBP occur with subsequent arrivals that are not present in the GBB recordings (e.g. Fig. 3a–d). These arrivals are characterized in the following paragraphs as surface waves. Moreover, the increase in the PGV and PGD at GBP with respect to the values observed at GBB is particularly marked for the strongest earthquakes. This may be due to an increase in the efficiency of the surface-wave generation process when the energy spectral content of the incident waves moves toward lower frequencies.

The PGA and PGV observed at GBP are compared with the peak ground motion predicted by the UMA05 (Bindi et al. 2006) for soft sites. The UMA05 attenuation relationships were derived for the Umbria-Marche region considering the strong motion data recorded during the 1997–1998 seismic sequence (SSN 2002). Therefore, the data recorded at GBP station and used in the present study were part of the data set used to derive the UMA05 models. The relationships were calibrated for

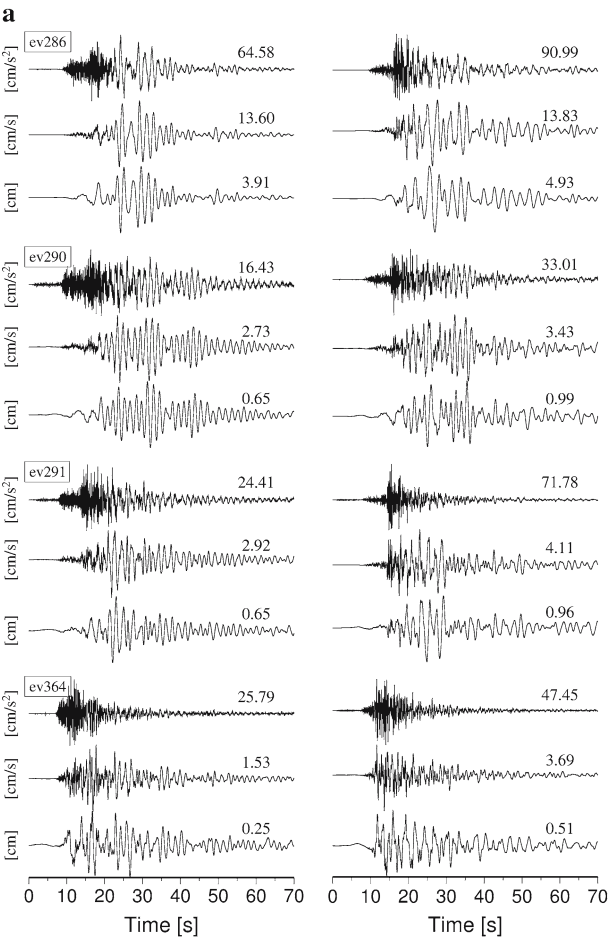

Fig. 2 **(a)** Normalized acceleration, velocity and displacement time series of earthquakes 286, 290, 291, and 364 (Table 1) recorded at GBP. The vertical (*Z*) and the north–south (*NS*) components are shown in the left and right panels, respectively. For each trace, the value of the maximum amplitude is noted. **(b)** The same as in Fig. 2a but for earthquakes 286, 291 and 364 (Table 1) recorded at GBB

peak ground acceleration, peak ground velocity and pseudo-velocity response spectra, grouping the stations used to derived UMA05 into four soil classes, accordingly to the thickness of the deposits and the average velocity of the upper 30 m. Figure 4 shows predicted and recorded PGA and PGV values for the eight events considered in this work (bottom frames) as well as the peak values for the magnitude 4.8 and 5.5 events versus epicentral distances (top and middle frames). The peaks at GBP are always higher than the predictions, with amplitudes that sometimes exceed the mean $+1\sigma$.

The complex structure of the bedrock morphology, characterized by strong lateral velocity variation, should certainly be considered when explaining the generation of the superficial waves and the corresponding peak amplitudes. However, the S-wave field also appears to be affected by the presence of the basin, causing high PGA values that are not predictable by standard attenuation relationships developed for soft sites.

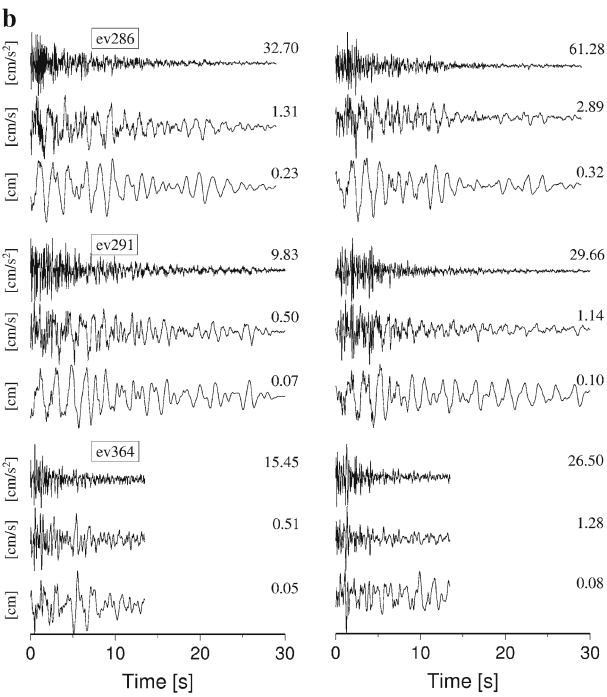

Fig. 2 continued

5 Frequency domain analysis

The spectral content of the GBP records is evaluated by means of the response spectra. Figure 5 shows the pseudo-velocity response spectra (5% damping) computed for GBP for events 286, 291 and 364, using different portions of the accelerogram. The first selected window contains the S-waves, the second one starts after the S-phase and includes the surface-wave arrivals (on average, this window is 25 s in length) and the last coincides with the total duration of the recording. The calculated horizontal and vertical spectra, found from the surface waves, for events 286 and 291 have their maxima centred at 0.6 Hz, and also show comparable peak amplitudes. The amplitude of the peaks related to surface waves appears to decrease with decreasing earthquake magnitude and, for event 364, has almost vanished. The response spectra calculated for the S-wave window do not show any resonant peak and the spectral ordinates at frequencies <1 Hz are much lower than those computed using the window that includes surface waves. The response spectra computed from the entire signal envelopes the spectra obtained from the two time windows. Figure 5 also compares the recorded pseudo-velocity response spectra at GBP and those computed from the UMA05 attenuation relationship for soft sites. For frequencies >1 Hz, the observed spectral ordinates are well described by the mean value plus one standard deviation, while they dramatically exceed the predicted values at frequencies <1 Hz for the 286 event. Again, we observe that the relevant low-frequency energy content is associated with the arrivals following the S-waves.

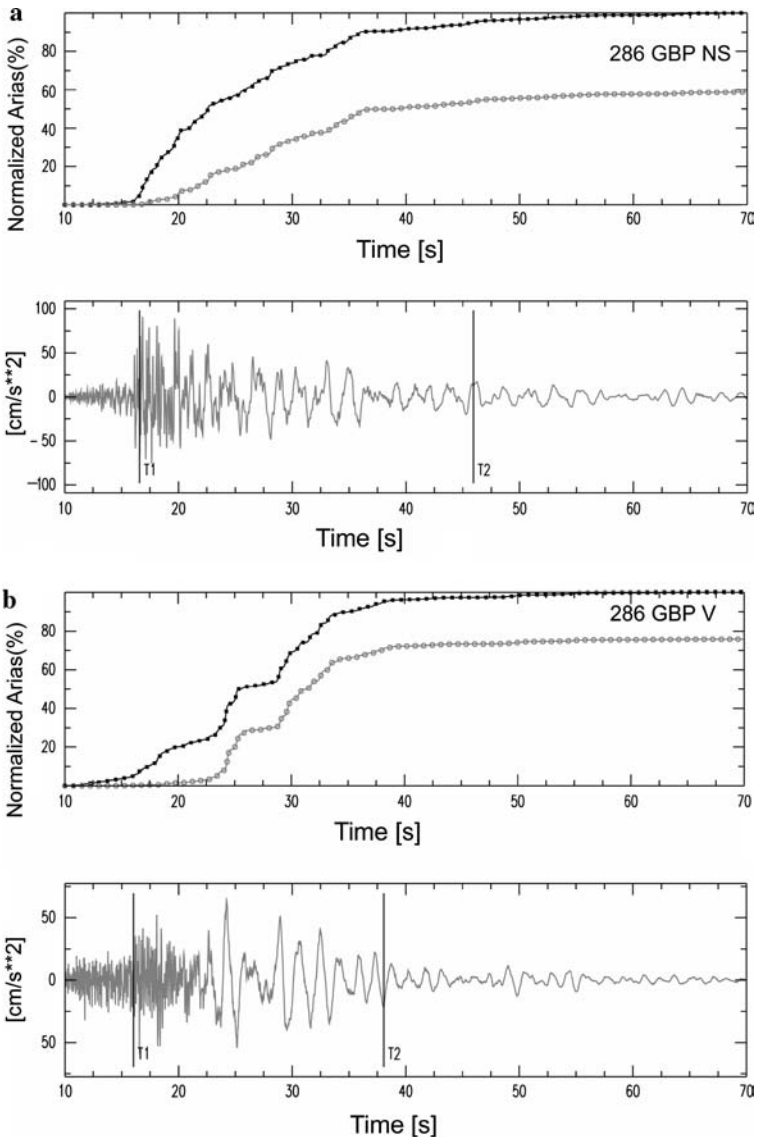

Fig. 3 **(a)** Arias intensity computed considering the NS component of event 286 at GBP. The Arias has been computed considering two different band pass filters, 0.2–40 Hz (*black line*) and 0.2–1.5 Hz (*grey line*). The duration T_1–T_2 is also shown (see text). **(b)** The same as in Fig. 3a but for the vertical component. **(c)** Arias intensity computed considering the NS component of event 286 at GBB. The Arias has been computed considering two different band pass filters, 0.2–40 Hz (*black line*) and 0.2–1.5 Hz (*grey line*). The duration T_1–T_2 is also shown (see text). **(d)** The same as in Fig. 3c but for the vertical component

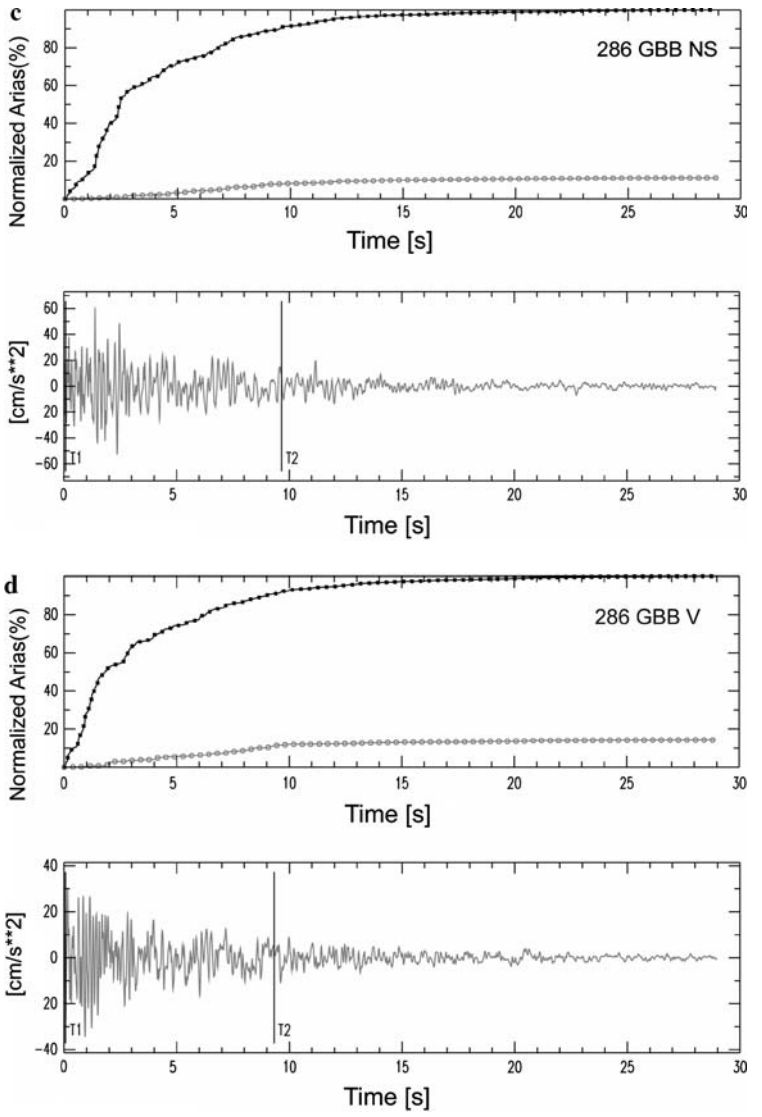

Fig. 3 continued

To evaluate the temporal variation of the spectral content of the GBP acceleration time series, spectrograms were computed using a moving window of 7 s length and overlapping for 6.5 s. As an example, the spectral analysis carried out for event 286 is shown in Fig. 6, although the main observations can be extended to all GBP recordings.

As shown in Fig. 6, middle panels, for the first 20 s, the energy is mainly contained at frequencies lower than 10 Hz, corresponding to the body wave arrivals. After the S-wave phase, the spectrograms show that the ground motion is dominated by strong low-frequency phases (<1 Hz) that persist for the duration of the recordings. These

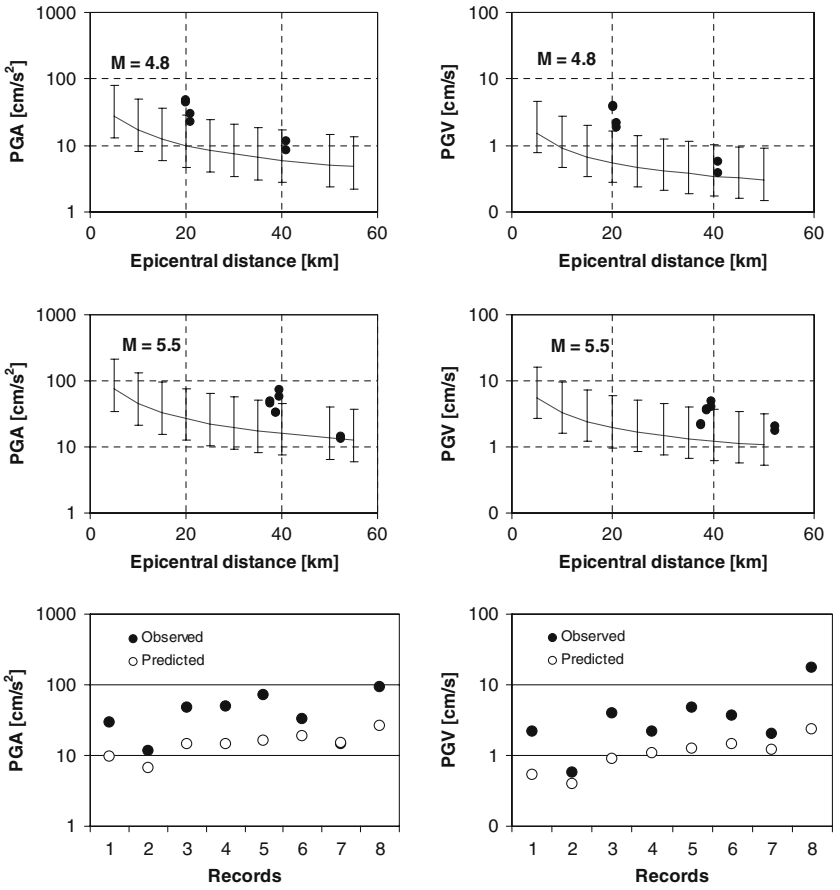

Fig. 4 Comparison between predicted PGV (*right*) and PGA (*left*) values against epicentral distance (Bindi et al. 2006) and the observed values at GBP, for two events, 353 (*top*) and 291 (*centre*). In the bottom panels, the predicted and observed PGA and PGV for all the earthquakes recorded at GBP (Table 1) are compared

phases affect the three components of ground motion, especially in the frequency range 0.4–0.8 Hz between 20 and 40 s. As suggested by other authors (Luzi et al. 2005, Bindi et al. 2005), the estimate of site amplification through vertical to horizontal spectral ratio at GBP is strongly dependent upon the selected time window and the corresponding waves included in the analysis. To highlight this point, Fig. 6 (bottom panels), shows the horizontal-to-vertical spectral ratio (HVSR, Lermo and Chavez-Garcia, 1993) variation with time computed considering the same moving window length and overlap as used for the spectrograms. The HVSR technique should be generally performed by averaging over several azimuth and distances. Although we apply this technique to only one recording at a time, the main HVSR variations with time provide useful insights into the characteristics of the site amplification at GBP. The HVSR mainly shows two amplification patterns: in the range 0.2–0.5 Hz and in the range 2.0–5.0 Hz, that persist for a long time. The former can be explained simply by considering the 1D amplification of the S-waves due to the soil column below the site,

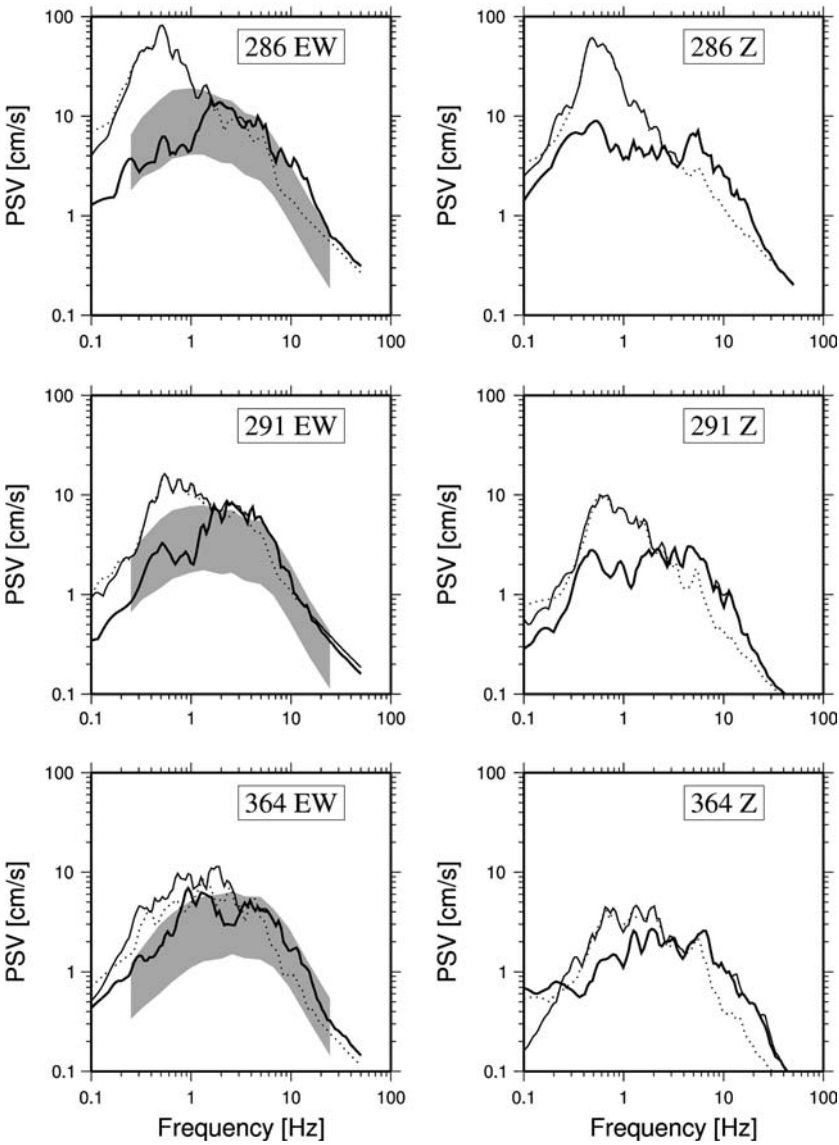

Fig. 5 Pseudo-velocity response spectra (5% damping) computed for events 286 (*top*), 291 (*centre*) and 364 (*bottom*) observed at GBP. The east–west and vertical components are shown in the left and right columns, respectively. Different windows of the accelerograms are considered for computing the response spectra: the S-waves window (*thin black lines*), the surface waves window (*dotted lines*), and the total duration of the recording (*thick black lines*). The grey areas indicate the spectral values between the mean $\pm 1\sigma$ predicted by the UMA05 relationships (Bindi et al. 2006)

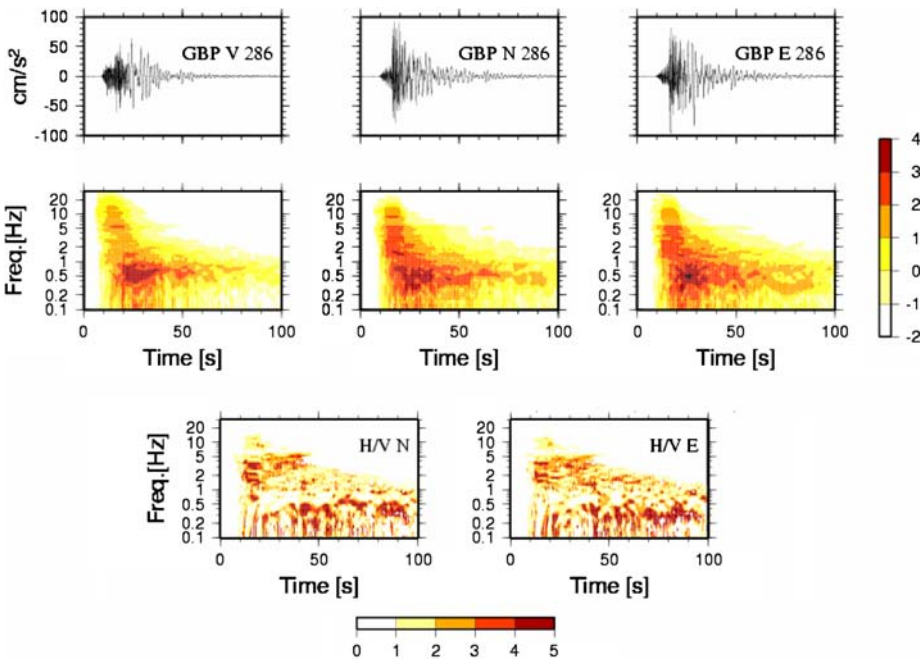

Fig. 6 Spectral analysis for event 286 recorded at GBP. *Top panels*: time series of the vertical (*left*), north–south (*centre*) and east–west (*right*) components. *Middle panels*: spectrograms in the frequency-time domain for the three components. *Bottom panels*: horizontal-to-vertical spectral ratio (*HVSR*) considering the north–south (*left*) and east–west (*right*) components

since it is consistent with the raw calculation based on the $\lambda/4$ approximation, assuming the S-wave velocity β=450 m/s and the bedrock depth $h \sim 300$ m (GE.MI.NA 1963). The latter corresponds to lower energy in the spectra of the recorded signal and may be due to the internal layering of the sedimentary structure. Conversely, the amplitudes of the HVSR assume values lower than 1 corresponding to the surface-wave arrivals at 20 s$< t <$40 s and 0.4 Hz$< f <$ 0.8 Hz, since these arrivals also affect the vertical component. In addition, we observe that, corresponding to the body-wave arrivals (10 s$< t <$20 s), the highest amplifications occur in the range 0.5–4 Hz for the north–south to vertical ratio and in the range 1–4 Hz for the east–west to vertical ratio. This, however, cannot be directly related to the 1D velocity profile below the station.

Next, we implemented the polarization analysis method proposed by Diallo et al. (2005), who extended the multi-component approach of Morozov and Smithson (1996) through the use of the wavelet transform. The instantaneous polarization attributes in the time-frequency domain are shown in Fig. 7a, for event 286 and frequencies lower than 1 Hz. Figure. 7a shows the instantaneous values of the ellipticity ratio (frame A), that is the ratio between the semi-minor axis and the semi-major axis of the ellipse corresponding to the particle motion (0 for a linearly polarized arrival and 1 for an elliptically polarized arrival), and of the angles between the planarity vector (Schimmel and Gallart 2003, Diallo et al. 2005) and the NS, EW and vertical (Z) components (frames B, C, and D, respectively). A value for these angles close to $\pi/2$ (red in Fig. 7a) means that most of the energy is incoming from the direction along the considered component. At frequencies <0.3 Hz, the energy is mostly con-

tained in the horizontal plane while for frequencies >0.3 Hz, it shows a greater vertical incidence. Between 20 and 40 s and for frequencies > 0.3 Hz, the dominant polarization is elliptical, suggesting the presence of Rayleigh waves. At ca. $t = 26$ s, a linearly polarized arrival lasts for about 6 s. Within this time interval (26–32 s), the incoming energy is contained in the horizontal plane for t <30 s, and in both the horizontal and the vertical components between 30 and 32 s. This behaviour indicates that different arrivals of Rayleigh and Love waves are recorded at the site. A linear polarization is observed again between 45 and 50 s, with energy mostly contained in the horizontal plane. We attribute this behaviour to a Love wave that is also clearly recognizable in the time series (Fig. 7b) and that appears to be responsible for the amplification shown by the HVSR in the range 0.5–1 Hz (Fig. 6, bottom panels). Summarizing, the polarization analysis clearly indicates the presence of both Love and Rayleigh waves and their complex propagation inside the basin. Without further investigation and modelling, the origin of the amplification patterns at GBP is not simply understood: the presence of the surface waves in the three components (not shown at the nearby rock station GBB) and the complex S-wave amplification works against a simple 1D explanation, suggesting that 2D, or even 3D, effects should be considered.

6 Discussion and conclusions

In this work we analysed the available accelerometric data recorded at the digital station GBP, located within an alluvial basin, and the analog station GBB, located at a nearby bedrock site located outside the basin. We applied time- and frequency-domain techniques and showed that the observed strong-ground motion parameters at GBP are affected by the presence of locally induced surface waves. The surface waves produce both a lengthening (by a factor of two) of the signal duration and an increase of the peak values, especially for PGV and PGD, with respect to station GBB. The basin-induced surface waves affect the three components of motion and their spectral content in the range 0.4–0.8 Hz. In particular, the vertical component carries the same amount of energy as the horizontal ones. A preliminary analysis showed that the polarization of the wave field, generated by the interference amongst the diffracted waves, strongly changes with time and frequency, due to the combination of Love and Rayleigh waves.

Differences between the two sites can be ascribed to a complex amplification phenomenon, related to both the stratigraphy below the GBP site (1D amplification effect) and to 2D/3D effects related to the complex morphology of the Gubbio basin. When attempts were made to estimate the response at GBP using classical techniques such as the H/V spectral ratio (HVSR), we partially captured the effects induced by the presence of a buried structure. However, the energy content at low frequencies carried by the surface arrivals, that can be seen as an energy increment with respect to the bedrock site, is not detectable. This is due to the 2D/3D effects that strongly affect the vertical component at the same frequencies as the horizontal motions, invalidating the hypotheses on which HVSR is based. For this class of site, other empirical techniques, rather than HVSR, should be considered to quantify at least the amplification frequency observed in the records.

In general, while the amplification effects related to the 1D transfer function are partially accounted for by the site coefficient introduced in the attenuation relationships, corrections for 2D/3D effects are not included in the standard functional. As a

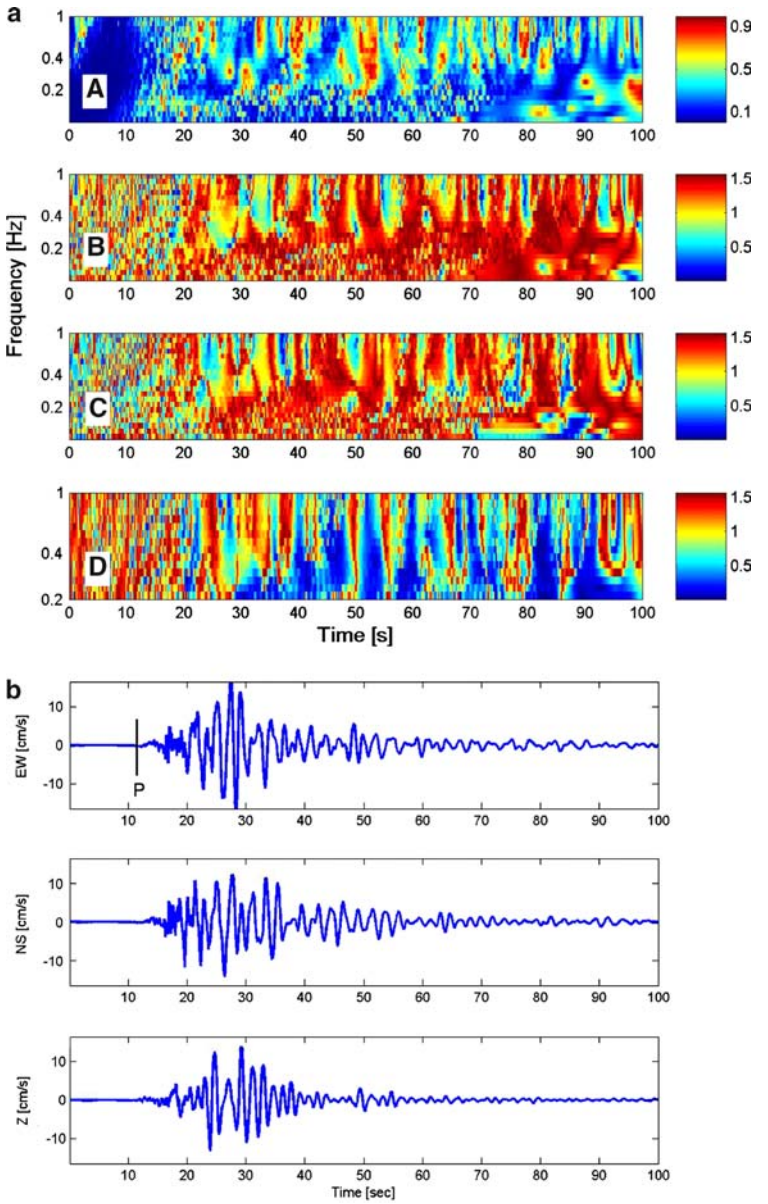

Fig. 7 **(a)** Instantaneous polarization attributes in the time-frequency domain of event 286 recorded at GBP: **A** ellipticity ratio, **B** the angle between the planarity vector and the NS direction, **C** the angle between the planarity vector and the EW direction, **D** the angle between the planarity vector and the vertical (Z) direction. **(b)** Time series of event 286 recorded at GBP and used for the polarization analysis shown in Fig. 7a

consequence, the strong ground-motion of a station such as GBP may not be correctly reproduced by classical attenuation relationships and specific local correction terms should be applied. To better assess the damage potential of the 2D/3D effects, the mechanism of surface wave generation and the response of the basin to their propagation must be studied in greater detail. To this aim, and to study the problem of introducing a specific amplification coefficient in the attenuation relationships for seismic hazard prediction, the installation of seismic arrays in Gubbio Piana is planned within the framework of a project funded by the Italian Dipartimento della Protezione Civile (DPC). Furthermore, the analysis of the data recorded by the seismic array can be used to study possible azimuthal dependence of the 2D/3D effects.

Acknowledgements Comments from two anonymous reviewers are acknowledged. This work has been partially funded by the Italian Dipartimento della Protezione Civile in the frame of the 2004–2006 agreement with Istituto Nazionale di Geofisica e Vulcanologia—INGV (project S3).

References

Ambraseys NN, Douglas J, Sarma SK, Smit PM (2005a) Equation for the estimation of strong ground motions from shallow crustal earthquakes using data from Europe and the Middle East: horizontal peak ground acceleration and spectral acceleration. Bull Earthquake Eng 3:1–53

Ambraseys NN, Douglas J, Sarma SK, Smit PM (2005b) Equation for the estimation of strong ground motions from shallow crustal earthquakes using data from Europe and the Middle East: vertical peak ground acceleration and spectral acceleration. Bull Earth Eng 3:55–73

Bindi D, Castro RR, Franceschina G, Luzi L, Pacor F (2004) The 1997–1998 Umbria-Marche sequence (Central Italy): source, path, and site effects estimated from strong motion data recorded in the epicentral area. J Geophys Res 109(B04312), DOI:10.1029/2003JB002857

Bindi D, Luzi L, Pacor F, Franceschina G, Castro RR (2006) Ground motion prediction from empirical attenuation relationships versus recorded data: the case of the 1997–1998 Umbria-Marche (Central Italy) strong motion data-set. Bull Seism Soc Am 96:984–1002, DOI:10.1785/0120050102

Castro RR, Anderson JG, Singh SK (1990) Site response, attenuation and source spectra of S-waves along the Guerrero, Mexico, Subduction Zone. Bull Seism Soc Am 80:1481–1503

Castro RR, Pacor F, Bindi D, Franceschina G, Luzi L (2004) Site response of strong motion stations in the Umbria region, Central Italy. Bull Seism Soc Am 94:576–590

Chavez-Garcia FJ, Faccioli E (2000) Complex site effects and building codes: making the leap. J Seism 4:23–40

Choi Y, Stewart JP, Graves RW (2005) Empirical model for basin effects accounts for basin depth and source location. Bull Seism Soc Am 94:1412–1427

Collettini C, Barchi MR, Chiaraluce L, Mirabella F, Pucci S (2003) The Gubbio fault: can different methods give pictures of the same object? J Geodyn 36:51–66

Diallo MS, Kulesh M, Holschneider, Scherbaum F (2005) Instantaneous polarization attributes in the time-frequency domain and wave field separation. Geophys Prospect 53:723–731

GE.MI.NA (1963) Ligniti e torbe dell'Italia Centrale. Geomineraria Nazionale, Torino, p319.

Graves RW, Pitarka A, Sommerville PG (1998) Ground motion amplification in the Santa Monica area: effects of shallow basin edge structure. Bull Seism Soc Am 88:1224–1242

Haskell NA (1953) The dispersion of surface waves on multilayered media. Bull Seism Soc Am 43:17–34

Hurby CE, Beresnev IA (2003) Empirical corrections for basin effects in stochastic ground-motion prediction, based on the Los Angeles basin analysis. Bull Seism Soc Am 93:1679–1690

Joyner WB (2000) Strong motion from surface waves in deep sedimentary basins Bull Seism Soc Am 90:S95–S112

Lermo J, Chavez-Garcia FJ (1993) Site effect evaluation using spectral ratios with only one station. Bull Seism Soc Am 83:1501–1506

Luzi L, Bindi D, Franceschina G, Pacor F, Castro RR (2005) Geotechnical site characterisation in the Umbria Marche area and evaluation of earthquake site-response. Pure Appl Geophs 162:2133–2161

Makra K, Raptakis D, Chavez-Garcia FJ, Pitilakis K (2001) Site effects and design provisions: the case of Euroseistest. Pure and Appl Geophs 158:2349–2367
Menichetti M (1992) Evoluzione Tettonico-Sedimentaria della valle di Gubbio. Studi Geologici Camertil: 155–163 (in Italian)
Mirabella F, Ciaccio MG, Barchi MR, Merlini S (2004) The Gubbio normal fault (Central Italy): geometry, displacement distribution and tectonic evolution. J Struct Geol 26:2233–2249
Morelli A, Ekstrom G, Olivieri M (2000) Source properties of the 1997–1998 central Italy earthquake sequence from inversion of long-period and broadband seismograms. J Seism 4:365–375
Morozov IB, Smithson SB (1996) Istantaneous polarization attributes and directional filtering. Geophysics 61:872–881
Olsen KB (2000) Site amplification in the Los Angeles basin from three-dimensional modelling of ground motion. Bull Seism Soc Am 90:S77–S94
Pucci, S, De Martini PM, Pantosti D, Valensise G (2003) Active tectonics in the Gubbio Basin (Central Italy): a contribution to the understanding of potential sources for damaging earthquakes in the area. Ann Geophys 46(5):837–864
Schimmel M, Gallart J (2003) The use of instantaneous polarization attributes for seismic signal detection and image enhancement. Geophys J Int 155:653–668
Sanchez-Sesma FJ, Ramos-Martinez J, Campillo M (1993) An Indirect Boundary Element method applied to simulate the seismic response of alluvial valleys for incident P, S and Rayleigh waves. Earth Eng Struct Dyn 22:279–295
SSN—Monitoring System Group (2002) The strong motion Records of Umbria-Marche sequence (September 1997 – June 1998). CD-ROM
Thomson WT (1950) Transmission of elastic waves through a stratified solid medium. J Appl Phys 21:89–93